European Review for Medical and Pharmacological Sciences 2022; 26: 3010-3024

Cinacalcet hydrochloride-nanoemulsion: preparation, characterization, enhanced bioavailability and pharmacodynamics

J. WANG[1], G.-G. CHEN[1], L.-L. REN[1,2]

[1]School of Pharmacy, Nanjing Tech University, Nanjing, China
[2]Department of Microbiology and Immunology, Stanford University, Stanford, CA, USA

Abstract. – OBJECTIVE: The aim of the study was to improve the bioavailability of Cinacalcet hydrochloride (CLC) and enhance its efficacy by the nanoemulsion drug delivery system.

MATERIALS AND METHODS: First, cinacalcet hydrochloride-nanoemulsion (CLC-NE) was prepared and optimized through the pseudo ternary phase diagram and central composite design response surface methodology (CCD). The release of CLC-NE *in vitro* was investigated with four different dissolution media, and the bioavailability of CLC-NE *in vivo* was studied through beagle dogs. Finally, the pharmacodynamics of CLC-NE was evaluated by the rat model of uremia.

RESULTS: Oleic acid, op-10, and PEG-200 were selected as oil phase, emulsifier, and co-emulsifier, respectively. The optimum ratio of oleic acid, op-10, PEG-200, and water was 9.87%, 38.33%, 12.78%, and 39.02%. CLC-NE has similar dissolution rates in different pH media, and the relative bioavailability of CLC-NE was 166.5%. The uremia model showed that CLC-NE could enhance renal function and reduce the excessive phosphorus (P), serum creatinine (Scr), and urea nitrogen (Urea) of model rats, as well as the inhibited increase of fibroblast growth factor-23 (FGF23) and parathyroid hormone (PTH).

CONCLUSIONS: The solubility, bioavailability, and pharmacodynamics of CLC can be significantly improved through the nanoemulsion drug delivery system.

Key Words:
Cinacalcet hydrochloride, Nanoemulsion, Solubility, Bioavailability, Pharmacodynamics.

Introduction

Chronic kidney disease (CKD) is a disease that seriously affects the normal life of human beings, second only to tumors, cardiovascular diseases, and diabetes[1]. With the increasing number of patients with metabolic syndrome, such as diabetes, obesity, and hypertension, the incidence of CKD increased year by year[2,3]. In the United States, CKD affects 11% of the population[4]. Secondary Hyperparathyroidism (SHPT) is a typical complication of CKD, and about 60% of patients who have just received dialysis will have SHPT[5-7]. SHPT is mainly caused by parathyroid tissue hyperplasia/adenoma formation and elevated serum PTH levels due to CKD[8]. The abnormal metabolism of calcium (Ca) and P, deficiency of vitamin D, reduced expression of the calcium-sensitive receptor in parathyroid cells, and skeletal resistance are all contributors to SHPT[9].

Since SHPT patients are characterized by excessive PTH secretion and parathyroid hyperplasia, controlling the disorders metabolism of Ca and P, reducing the secretion of PTH, and increasing gland volume are regarded as the effective treatment for SHPT[10-12]. Now, SHPT is mainly treated by phosphorus binder or vitamin D supplement[13], which only works for some time, and the condition is prone to repeat[14].

CLC, a calcium-sensitive receptor (CaSR) agonist, can effectively treat SHPT[15,16] by inhibiting PTH by binding to the transmembrane domain of the surface and transferring quasi calcium signals to cells. Despite the clear efficacy of CLC on SHPT, the extremely low solubility in water (38.6 μg/ml) greatly limits its therapeutic efficacy on SHPT[17]. The existing CLC dosage forms on the market are tablets with poor oral absorption[18-20]. The solid dispersion of CLC has also been reported in the literature, which will precipitate in the long-term storage and affect the efficacy of CLC[21]. Preparing CLC into a dosage with high solubility and good stability has become an urgent need.

Corresponding Authors: Lili Ren, MD; e-mail: renlili@njtech.edu.cn
Guoguang Chen, MD; e-mail: guoguangchen@163.com

Nanoemulsion, a special equilibrium system for the formation of the aqueous phase, oil phase, emulsifier, and co-emulsifier, has low viscosity, isotropic properties, and thermodynamic and kinetic stability[22-24]. While drugs were made into nanoemulsions, the solubility of insoluble drugs can be increased[25], as well as the stability of water-soluble drugs[26]. Nanoemulsions provides an option for CLC[27-29].

In this paper, CLC-NE was prepared by the phase inversion method. The optimal prescription was screened through the pseudo ternary phase diagram and CCD. Then, the release of CLC-NE *in vitro* was investigated with four different dissolution media, and the bioavailability of CLC-NE *in vivo* was studied through beagle dogs. Finally, the Uremic rats (UR) model was established by removing 5/6 of the kidneys of rats and combining with a high phosphorus diet, which was used to study the pharmacodynamics of CLC-NE.

Materials and Methods

Materials

We used cinacalcet hydrochloride (Jiangsu Hausen Pharmaceutical Co., LTD., Lianyungang, Jiangsu Province, China), REGPARA® (Kyowa Hakko Kirin Co., Ltd, Chuo District, Tokyo, Japan).

Screening of Oil Phase, Emulsifier, and Co-Emulsifier

The optimal preparation of nanoemulsion was selected by the solubility of CLC. Oil phase: castor oil, ethyl oleic acid, methyl oleate, and oleic acid[30,31]; emulsifier: OP-10, Tween-80, Span-80, and glycerol triacetate[32]; co-emulsifier: ethylene glycol[33], propylene glycol[34], PEG-200 and PEG-400[35,36]. After 3 mL of the aforementioned different excipients and excess CLC were added to 10 mL centrifuge tubes and, sonicated for 5 min. After shaking at 200 rpm for 24h at 37°C, the supernatant was centrifuged, diluted with methanol, and analyzed by HPLC. The chromatographic system (Shimadzu, Kyoto, Japan) was purchased from Japan. 20 μL volume of samples were injected into a Phenomenex C18 Column (4.6×250 mm, 5 μm) and the detection wavelength was 272 nm. The flow rate was 1.0 mL/min with an 85:15 (v/v) mixture of methyl alcohol and triethylamine aqueous solution (pH 8.0) at 30°C. Each sample was determined three times in parallel.

Table I. The test design of CCD.

Serial number	X_1 (%)	X_2 (%)
1	10.00	65.00
2	5.00	65.00
3	15.00	35.00
4	10.00	50.00
5	5.00	35.00
6	10.00	50.00
7	17.07	50.00
8	10.00	50.00
9	10.00	50.00
10	10.00	50.00
11	15.00	65.00
12	5.00	50.00
13	10.00	35.00

Pseudo-Ternary Phase Diagram

The ratio of emulsifier and co-emulsifier (km) is set as 1:1, 1:2, 1:3, and 1:4, and the two are mixed in these four proportions to form a mixture (Smix). We added the oil phase to Smix in the ratio of 1:9, 2:8, 2:8, 3:7, 4:6, 5:5, 6:4, 7:3, 8:2, 9:1, and stirred at the same speed. After being mixed evenly, distilled water is dropped into the mixture until the nanoemulsion is formed to calculate the amount of each phase. The km values were determined by drawing the pseudo-ternary phase diagram with the oil phase, water, and Smix as the vertices. The mixture was evenly mixed and distilled water was dropped into the mixture until the nanoemulsion was formed to calculate the amount of each phase.

CCD

After determining the ratio of emulsifier to co-emulsifier, the specific proportion of oil phase, water phase, emulsifier, and co-emulsifier in CLC-NE was determined by CCD. The CLC content is fixed at 2.5% (w/w), while the proportion of oil phase (X_1) ranges from 5% to 15% and the proportion of Smix (X_2) ranged from 35% to 65%. The particle size (Y_1) and polydispersion index (PDI) (Y_2) of nanoemulsion were used as screening criteria, and the software Design-Expert.v8.0.6.1 was used to design and optimize the experiment (Table I).

Preparation of CLC-NE

The optimal prescribed amount of Smix and oil phase were added to the round bottom flask, mixed evenly, and CLC was added. The mixture was stirred at 37°C until CLC was completely dissolved. Then, distilled water was added, and the solution was stopped with light blue light,

which indicates the successful preparation of CLC-NE.

Characterization of CLC-NE

Particle size, polydispersion index (PDI), and Zeta potential

CLC-NE was diluted 50, 100, and 1,000 times with distilled water. The particle size of CLC-NE at different dilutions was determined with a Zatasizer 3000 Hs granulometer (Malvin Panalytical Co., Ltd, Malvern, UK), as well as the PDI and the Zeta potential of CLC-NE diluted 100 times. Each sample was tested in parallel three times.

Transmission electron microscope (TEM)

CLC-NE was diluted 100 times, dropped onto the copper web, and stained with 2% sodium phosphotungstate. After the samples were dried, the shape and particle size of CLC-NE were observed by EM-05500TGP transmission electron microscope (JEOL Japan Electronics Co., Ltd, Showa, Tokyo, Japan).

Stability of CLC-NE

To investigate the stability of CLC-NE, the particle size and PDI were studied by diluting CLC-NE with different pH media. CLC-NE was diluted 50, 100, and 1000 times with water, pH1.2 hydrochloric acid solution, pH4.5 acetate buffer, and pH6.8 phosphate buffer, respectively. The particle size and PDI of the sample were measured after 24h at room temperature to determine whether pH and dilution could affect CLC-NE.

Dissolution in Vitro

The solubility of CLC-NE *in vitro* was performed by the dialysis bag method with CLC as the contrast. The dissolution mediums were pH1.2 hydrochloric acid solution, pH4.5 acetate buffer, and pH6.8 phosphate buffer. CLC and CLC-NE were configured at the concentrations of 250 μg/mL with dissolution mediums, 1 mL was added to the dialysis bag and both ends were closed. 500 mL dissolved mediums were preheated to 37°C and dialysis bags containing CLC, and CLC-NE were placed. The mixture was stirred at 50 rpm and supplemented with 5 mL samples at 5, 10, 15, 20, 30, 45-, 60-, 90-, and 120-min. Samples were analyzed by HPLC and *in vitro* dissolution curves for CLC-NE and CLC. The mixture was stirred at 50 rpm, sampling 5 mL at 5, 10, 15, 20, 30, 30, 45, 60, 90, 120 min, and supplemented with an equal volume of dissolution medium. Samples were analyzed by HPLC to plot the dissolution curves of CLC-NE and CLC *in vitro*.

The similarity of the dissolution curves of CLC-NE in different dissolution mediums was investigated by similarity factors (f_2, Formula 1). When f_2 >50, the two curves were considered to be similar.

$$f2 = 50 * \lg\left[100/\sqrt{1 + \frac{\sum_{i=1}^{n}(Ti-Ri)^2}{n}}\right] \quad (1)$$

In the formula, Ti and Ri are the dissolutions of CLC-NE at each sampling time point in different media, and n is the number of sampling points.

Pharmacokinetic Study

All animal experiments were carried out with the permission of the Nanjing Medical University Institutional Animal Care and Use Committee (No. 202009107). Eight beagles were randomly divided into two groups (half male and half female in each group) and were fasted for 12h. One group received oral administration of REGPARA® and the other group was orally administered CLC-NE. 4 mL of blood was taken from the forelimb vein at 0.5, 1, 1.5, 2, 3, 4, 6, 8, 10, 12, and 24h after administration with heparin sodium tube. After homogenization, the blood was centrifuged at 4000 rpm for 5 min. The plasma was taken and stored in a 10 mL centrifuge tube at -20°C. One week later (CLC cleared in beagles), two groups of beagles were switched, and the procedure was repeated.

50 μL fluoxetine (3 μg/mL, internal standard) and 5 mL extractant (diethyl ether: Dichloromethane =7:3) were added to 1 mL plasma, mixed for 5 min and centrifuged at 4000 rpm for 5 min to take the supernatant. Then, 5 mL extractant was added and the procedure was repeated.

Two supernatants were combined, dried by a nitrogen blower at 50°C, redissolved with 200 μL methanol, and centrifuged at 13000 rpm for 5 min to take supernatants, which were analyzed by HPLC. Data were processed with the software DAS 2.0.

Pharmacodynamics Study

40 male SD rats were divided into two groups with 10 rats in the sham-operated group (Sham group) and 30 rats in the model group. Rats in the model group were fasted for 8h before surgery, and intraperitoneal injected with 10% chloral hydrate (3.6 mL/kg) for anesthesia. A 1 cm incision

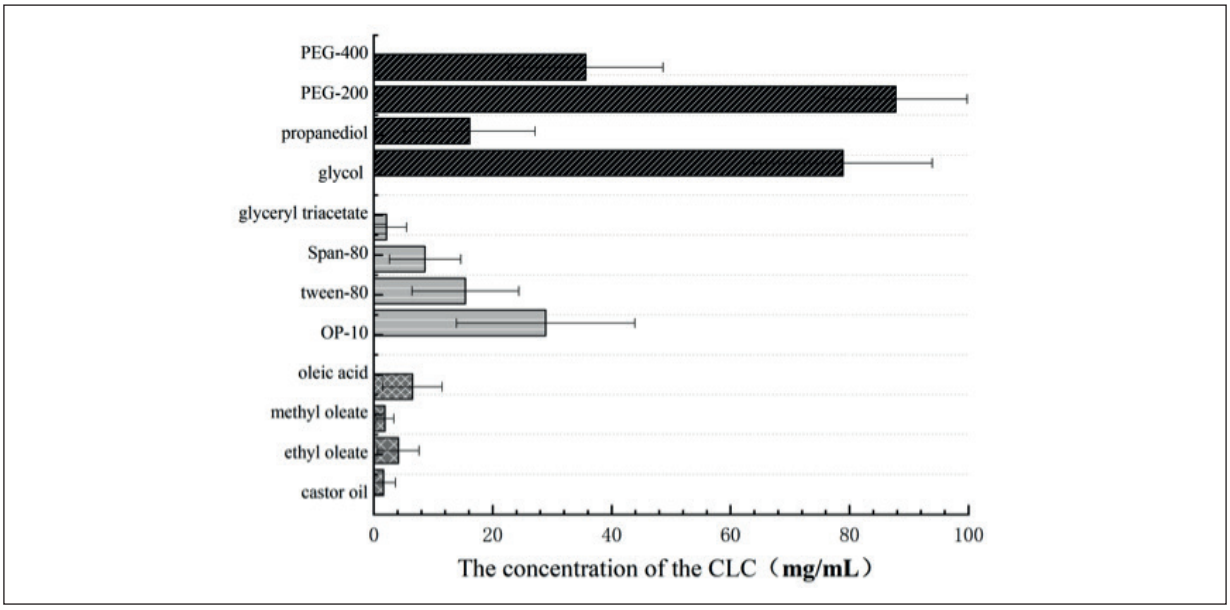

Figure 1. The solubility of CLC in different oils, surfactants, and co-surfactants (n=3).

under the left rib of the rat was made, the kidney envelope was removed from the incision, as well as 1/3 of the upper and lower of the left kidney, respectively. The wound was pressed to stop bleeding and sutured. One week later, the same operation was performed to remove the right kidney and the 5/6 NR model was established. Rats in the sham-operated group were only removed the kidney envelope on both sides. The experiment began 4 weeks after feeding high-phosphorus food daily.

Rats in the model group were divided into three groups, including the 5/6 nephrectomy rat+saline (NR +saline), the 5/6 nephrectomy rat+CLC (NR+CLC), and the 5/6 nephrectomy rat+CLC-NE (NR+CLC-NE). Rats in the NR+CLC group were given CLC (10 mg/kg) intragastrically every day, while rats in the NR+-CLC-NE group were given CLC-NE (containing 10 mg/kg of CLC) intragastrically. The other rats (rats in the Sham group and the NR+saline group) were administered with isovolumetric saline. High-phosphorus foods were fed during the experiment. 0.8 mL blood was collected from the orbital vein of all rats at the 0 and 6 weeks of the experiment, which was left standing at room temperature, centrifuged at 5000 rpm for 10 min to collect the serum.

The contents of SCr, Urea, Ca, and P were detected by Indiko automatic biochemical analyzer (Thermo Fisher Scientific, Waltham, MA, USA), while 25(OH)D_3 was detected by Roche 16101 electrochemical method. PTH and FGF23 were detected by Elisa.

Statistical Analysis

All statistical analyses were performed using Origin 8.6. All results are shown as the mean ± standard deviation (M±SD). A p-value <0.05 was considered significant.

Results

Screening of Oil Phase, Emulsifier, and Co-Emulsifier

A higher the solubility of the API in the excipient determined a more stable the prepared nanoemulsion[37]. The solubility of CLC in different excipients was shown in Figure 1. Among the four oil phases, CLC had the highest solubility in oleic acid, which was selected as the oil phase. The emulsifier is OP-10 with the highest solubility of CLC, and the co-emulsifier is PEG-200.

Pseudo-Ternary Phase Diagram

The co-emulsifier can regulate the Hydrophile-Lipophile Balance Number (HLB) of the emulsifier[38] and intervene in the interface membrane of the emulsifier to form a composite con-

densed film, which can improve the firmness and flexibility of the membrane, as well as the solubility of the emulsifier[39]. Km determines the formation of nanoemulsions. Km was fixed and the proportion of Smix to oil phase was adjusted to prepare nanoemulsions (Figure 2). When km=3:1, nanoemulsions can be formed in more conditions, so the ratio of the emulsifier to the co-emulsifier is determined to be 3:1.

CCD

The experiment was carried out according to the design of CCD (Table I), and the results were analyzed by CCD. ANOVA showed that *p*-values of Y1 and Y2 were both less than 0.05, indicating significant differences between models. R^2 were 0.9497 and 0.9487 respectively, indicating a good correlation between independent variables and dependent variables. After regression analysis of the test data, the quadratic multiple regression equation can be obtained (Formula 2 and Formula 3):

$$Y_1=22.36+0.69X_1-3.55X_2+0.22X_1X_2+17.67X_1^2+15.45X_2^2 \quad (2)$$

$$Y_2=0.22+3.016*10^{-3}X_1+2.691*10^{-3}X_2+2.5*10^{-4}X_1X_2+0.039X_1^2+0.055X_2^2 \quad (3)$$

The 3D response surface plots and contour plots of the particle size and PDI of the CLC-NE prepared under different conditions are shown in Figure 3. While the content of the oil phase was fixed, the particle size of CLC-NE (Figure 3A) and PDI (Figure 3B) first decreased, and then, increased with the increased content of Smix. The optimal prescription of CLC-NE calculated by CCD is oil phase content 9.87%, emulsifier content 38.33%, co-emulsifier content 12.78%, and aqueous phase content 39.02%.

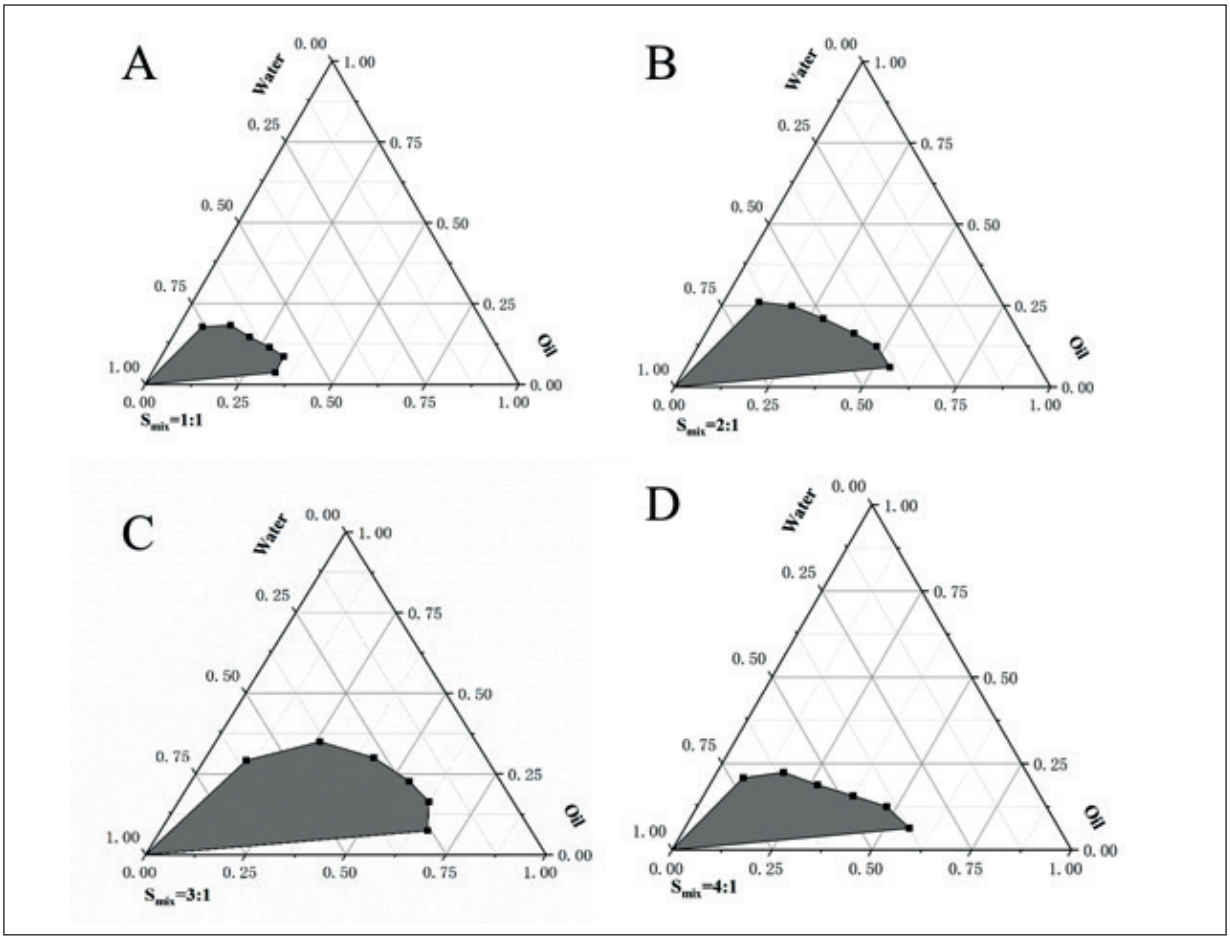

Figure 2. The pseudo-ternary phase diagram of different value of Km. **A**, Km=1:1; **B**, Km=2:1; **C**, Km=3:1; **D**, Km=4:1.

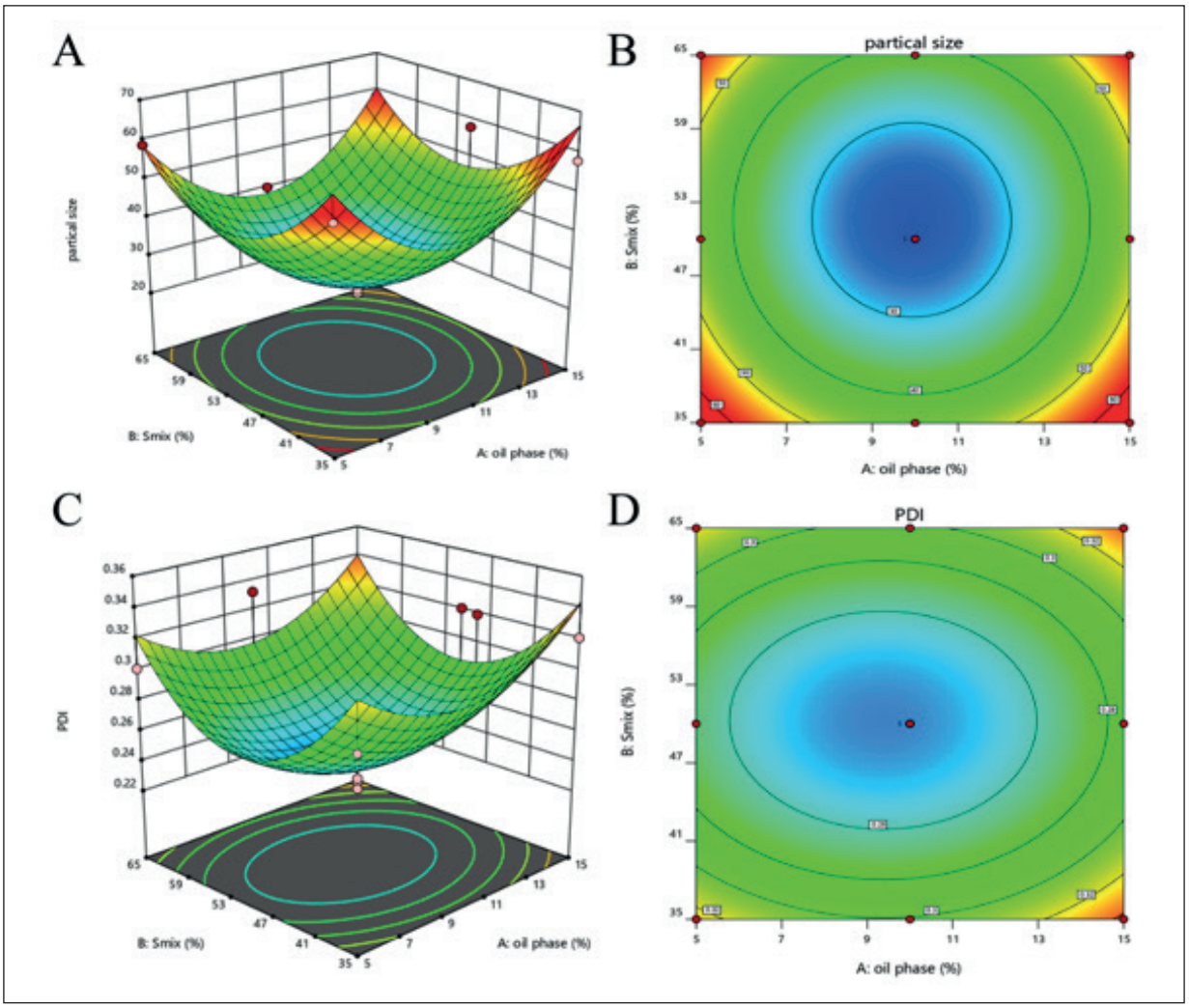

Figure 3. The effect of the content of oil and S_{mix} on the particle size and PDI of nanoemulsion. ***A-B***, Particle size; **C**, and **D**, PDI.

Characterization of CLC-NE

Particle size, PDI, and Zeta potential

The particle size distribution of CLC-NE was detected by a Zatasizer 3000 Hs granulometer (Malvin Panalytical Co., Ltd, Malvern, UK), with an average particle size of 24.1±3.8 nm (Figure 4) and PDI of 0.261±0.032. The Zeta potential of CLC-NE was -26.56±0.67 mV, and its absolute value is greater than 20, indicating the good stability of the system[40]. The negative charge of CLC-NE may be caused by the free fatty acids.

TEM

CLC-NE was diluted 100 times and observed by TEM, which was shown in Figure 5. CLC-NE is spherical with a distinct putamen structure, and the particle size is less than 100 nm, which is consistent with the particle size measured above. By comparing the diffusion rate of water-soluble dye (methylene blue) and oil-soluble dye (Sudan III) in CLC-NE, we found that the diffusion rate of methylene blue was significantly faster than that of Sudan III, indicating that CLC-NE is a nanoemulsion of type O/W and the core of TEM is the oil phase containing CLC.

Stability of CLC-NE

CLC-NE was diluted 50, 100, and 1,000-fold by purified water, pH1.2 hydrochloric acid solution, pH4.5 acetate buffer, and pH6.8 phosphate buffer, respectively. The particle size and PDI of the CLC-NE were not significantly altered after 24h at room temperature (Table

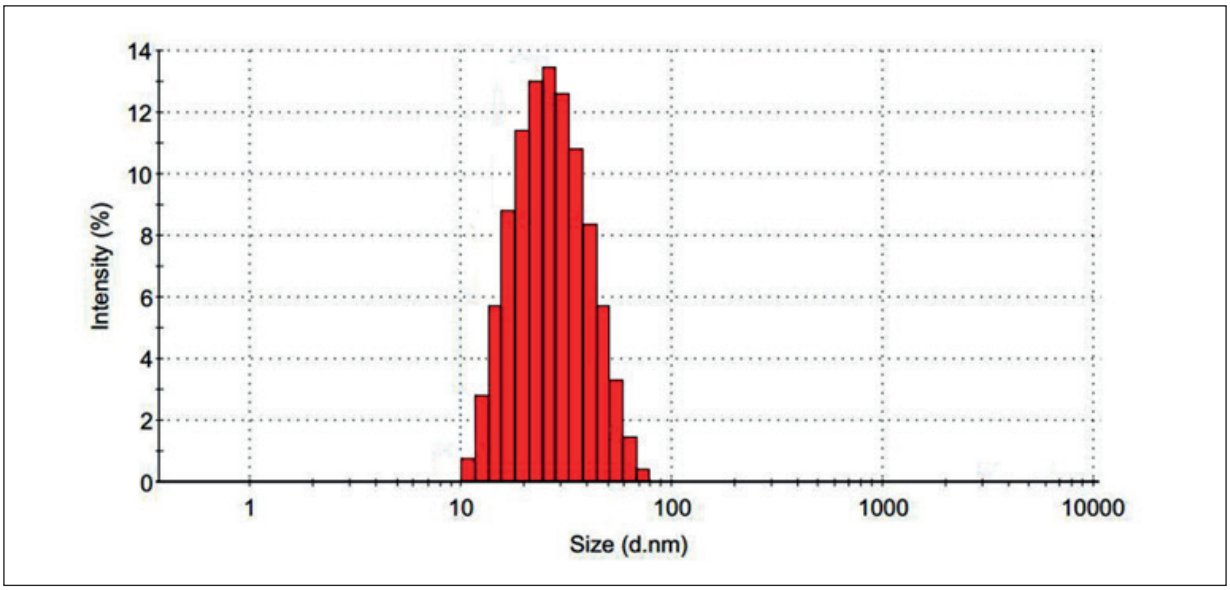

Figure 4. The size distribution of CLC-NE.

II), and no flocculation, precipitation, or phase transition occurred.

Dissolution In Vitro

As can be seen from Figure 6, the dissolution of CLC was significantly affected by pH, with only 38.2% and 50.1% dissolution in pH6.8 phosphate buffer and water. However, CLC-NE showed completely different dissolution characteristics. In the four media, the cumulative dissolution of CLC-NE reached more than 85% at 60 min and about 90% at 120 min. The dissolution curves of CLC-NE in pH1.2 hydrochloric acid were used as the reference to calculate the f_2 of the dissolution curves in the four media. The f_2 of CLC-NE in pH4.5 acetic acid buffer, pH6.8 phosphate buffer, and water were 67, 82, and 75, respectively, all greater than 50, indicating that the dissolution curves of CLC-NE in the four media were similar, and the dissolution of CLC-NE was not affected by pH.

Pharmacokinetic Study

REGPARA® was used as a positive drug to compare the bioavailability of CLC-NE and CLC in beagles (Figure 7 and Table III).

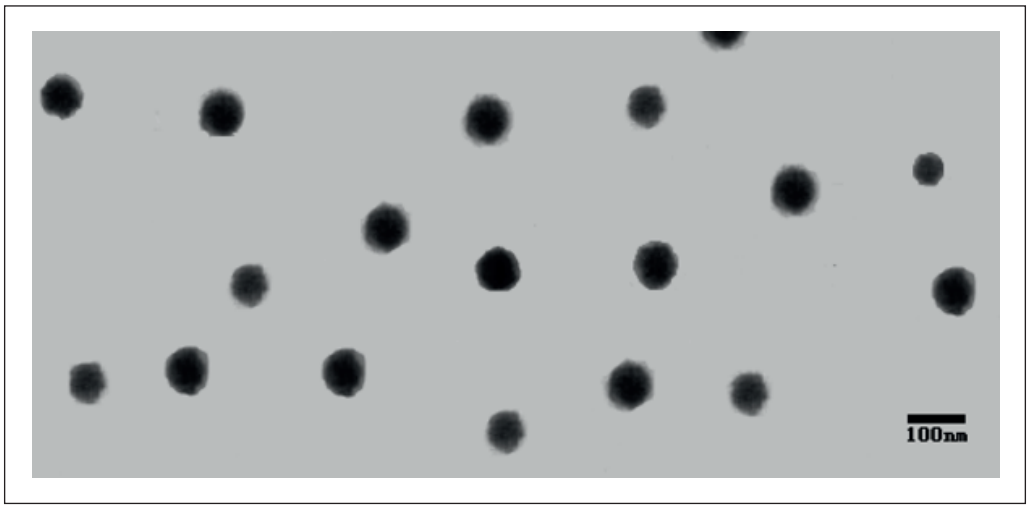

Figure 5. TEM image of CLC-NE with 100-fold dilution.

Table II. The influence of different medium and diluted multiples (n=3).

Medium	Dilution ratio	Particle size (nm)		PDI	
		0h	24h	0h	24h
pH1.2 hydrochloric acid solution	50	23.7±3.8	24.1±3.6	0.292±0.018	0.258±0.021
	100	24.9±5.1	26.2±4.5	0.236±0.031	0.137±0.033
	1000	24.1±3.6	25.6±2.9	0.198±0.026	0.202±0.029
pH4.5 acetate buffer	50	23.6±2.9	23.2±4.8	0.168±0.045	0.196±0.023
	100	25.8±3.2	26.5±3.9	0.253±0.037	0.227±0.019
	1000	24.5±4.0	25.9±5.1	0.191±0.028	0.175±0.036
pH6.8 phosphate buffer	50	25.1±2.6	27.3±6.9	0.238±0.013	0.182±0.027
	100	24.7±3.4	23.9±5.3	0.217±0.030	0.178±0.032
	1000	24.7±3.9	24.8±4.6	0.172±0.027	0.206±0.022
Water	50	24.8±4.2	23.9±5.1	0.229±0.032	0.253±0.029
	100	23.9±3.8	25.2±4.9	0.275±0.018	0.189±0.035
	1000	24.1±3.3	26.4±5.6	0.183±0.032	0.211±0.027

CLC-NE was absorbed rapidly after oral administration, with a T_{max} of 2.88±0.35h, which was similar to REGPARA® (2.13±0.35h). However, the maximum plasma concentration (C_{max}) of CLC-NE was much higher than that of REGPARA® (155.91±6.11 ng/mL and 107.36±3.34 ng/mL), indicating that nanoemulsion can significantly improve the plasma concentration of CLC *in vivo*. The AUC ($_{0\text{-}\infty}$) of REGPARA® was used as a reference, and the relative bioavailability of

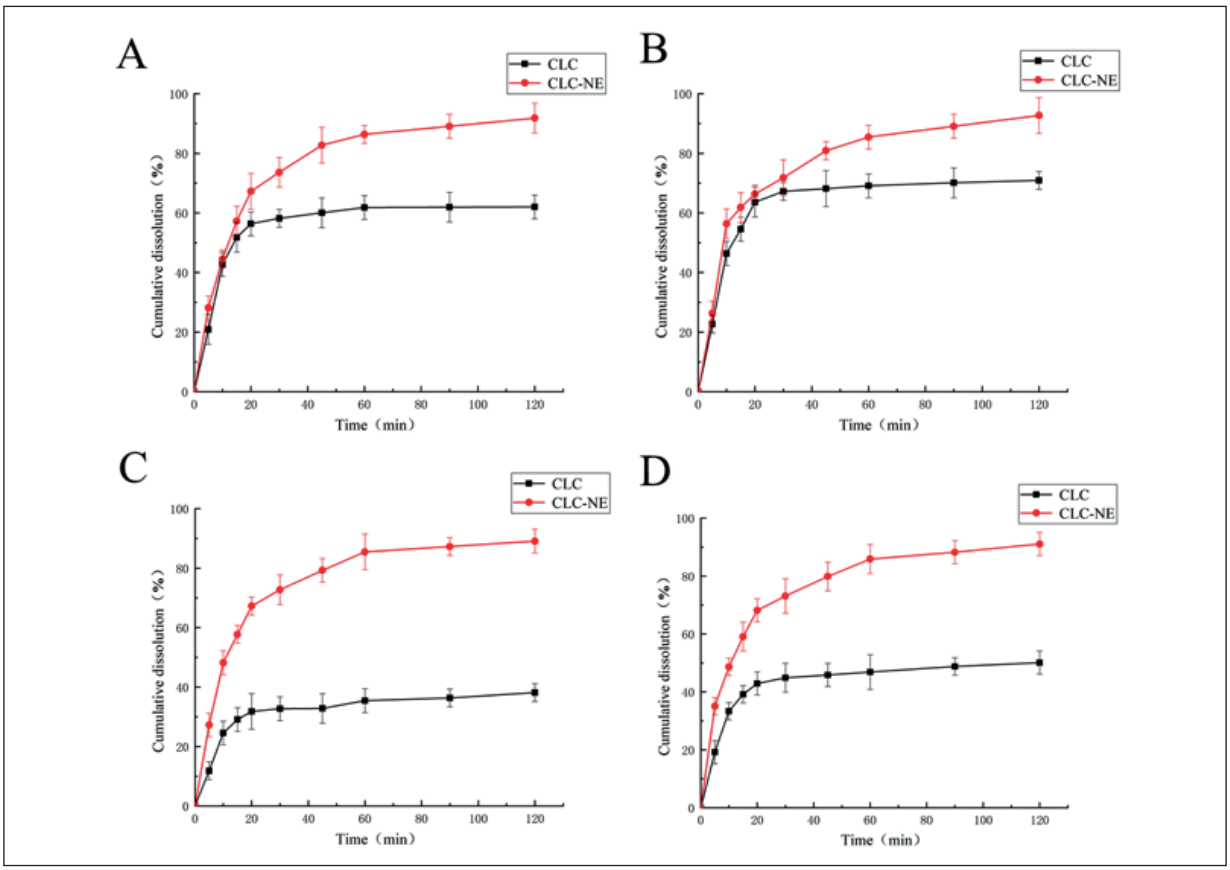

Figure 6. The dissolution profiles of CLC commercial tablets and CLC-NE in four different media. **A**, pH1.2 hydrochloric acid. **B**, pH4.5 acetate buffer. **C**, pH6.8 phosphate buffer. **D**, Water.

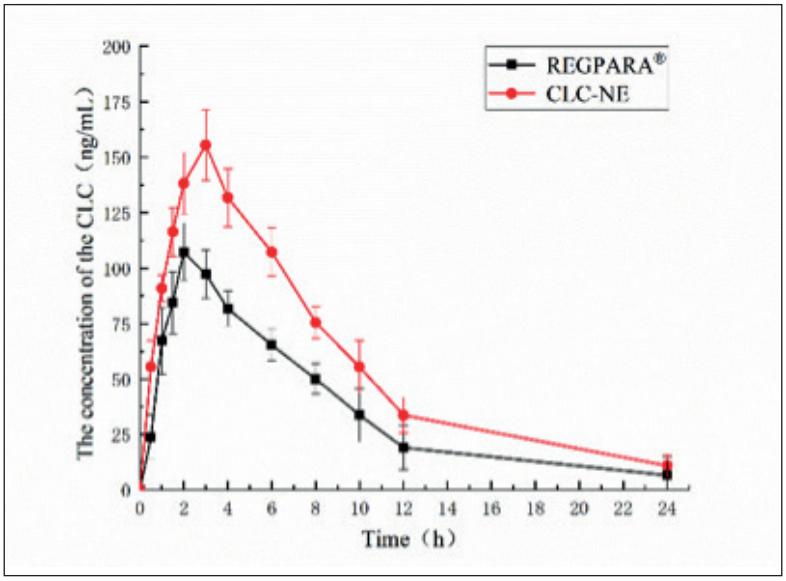

Figure 7. The profile of the mean plasma drug concentration-time of CLC-NE.

CLC-NE was calculated to be 166.50%, significantly higher than that of REGPARA®.

Pharmacokinetic Study

The body weight changes of rats 6 weeks after administration were shown in Figure 8. The hair of the Sham group was shiny, and the bodyweight increased normally (from 240.51 g to 357.06 g). However, rats in the NR+saline group had dull hair, slow response, and significantly less weight than rats in the Sham group (263.42 g *vs.* 357.06 g). After intragastric administration of CLC-NE, the weight gain of the rats was higher than that of the rats with saline and CLC, reaching 316.93 g,

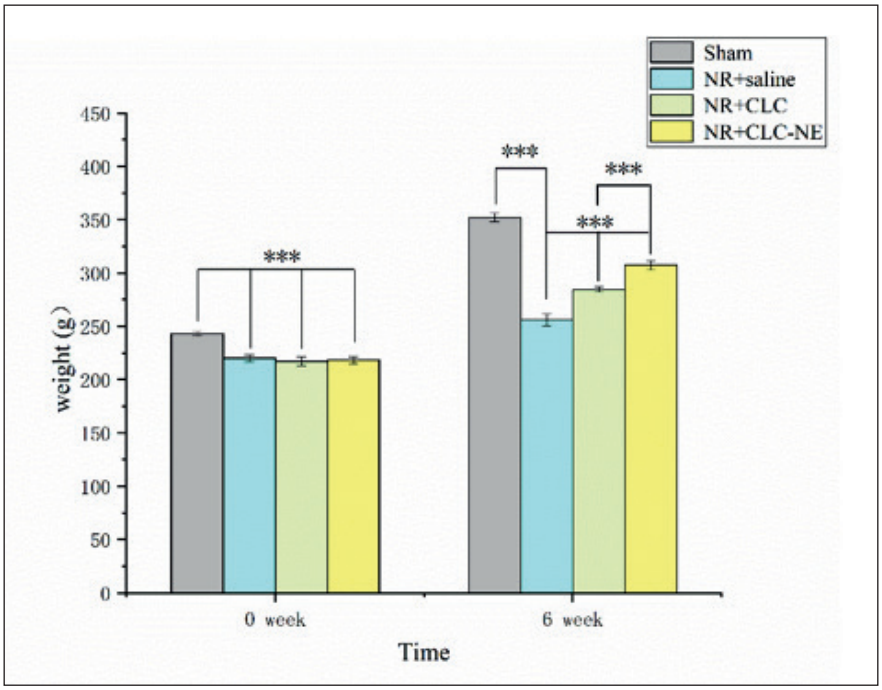

Figure 8. Weight changes of rats in different groups (Sham group, NR rats+ saline group, NR rats + CLC, NR rats + CLC-NE) during the 6-week treatment (Mean values ± SD, n=10, ***p<0.001).

Table III. Pharmacokinetic parameters of CLC-NE (n=8).

Parameter	REGPARA®	CLC-NE
C_{max} (ng/mL)	107.36±3.34	155.91±6.11*
T_{max} (h)	2.13±0.35	2.88±0.35
$AUC_{(0-t)}$ (ng/mL*h)	705.63±9.95	1098.45±26.04*
$AUC_{(0-\infty)}$ (ng/mL*h)	811.89±38.58	1350.29±79.71*
Relative bioavailability (%)	100.00	166.50

*p<0.05 compared with REGPARA®.

indicating that CLC-NE has a therapeutic effect on NR and is better than CLC.

Scr and Urea are measures of kidney function[41-43]. After 5/6 of the kidneys were removed from NR, the renal function of rats decreased, resulting in the increasing of serum SCr and Urea. Therefore, the serum Scr (101.88 umol/L) and Urea (15.69 mmol/L) in the NR+ Saline group (Figure 9A and 9B) were higher than those in the Sham group (Scr 20.63 umol/L and Urea 6.85 mmol/L), indicating that the model was successfully established. After intragastric administration of CLC-NE and CLC, renal function of rats recovered and serum Scr and Urea of NR decreased. Due to the low solubility and bioavailability of CLC, serum Scr (107.75 umol/L) and Urea (19.67 mmol/L) of rats in the NR+CLC group were significantly higher than those of rats in the NR+CLC-NE group (62.13 umol/L and 12.30 mmol/L), which suggests that CLC-NE can promote the uptake of CLC in rats and exert stronger efficacy. Meanwhile, the excessive serum P of NR was also inhibited with the intragastric administration of CLC-NE and CLC (Figure 9C), which was significantly lower than that of NR+saline. Moreover, CLC-NE showed a stronger inhibi-

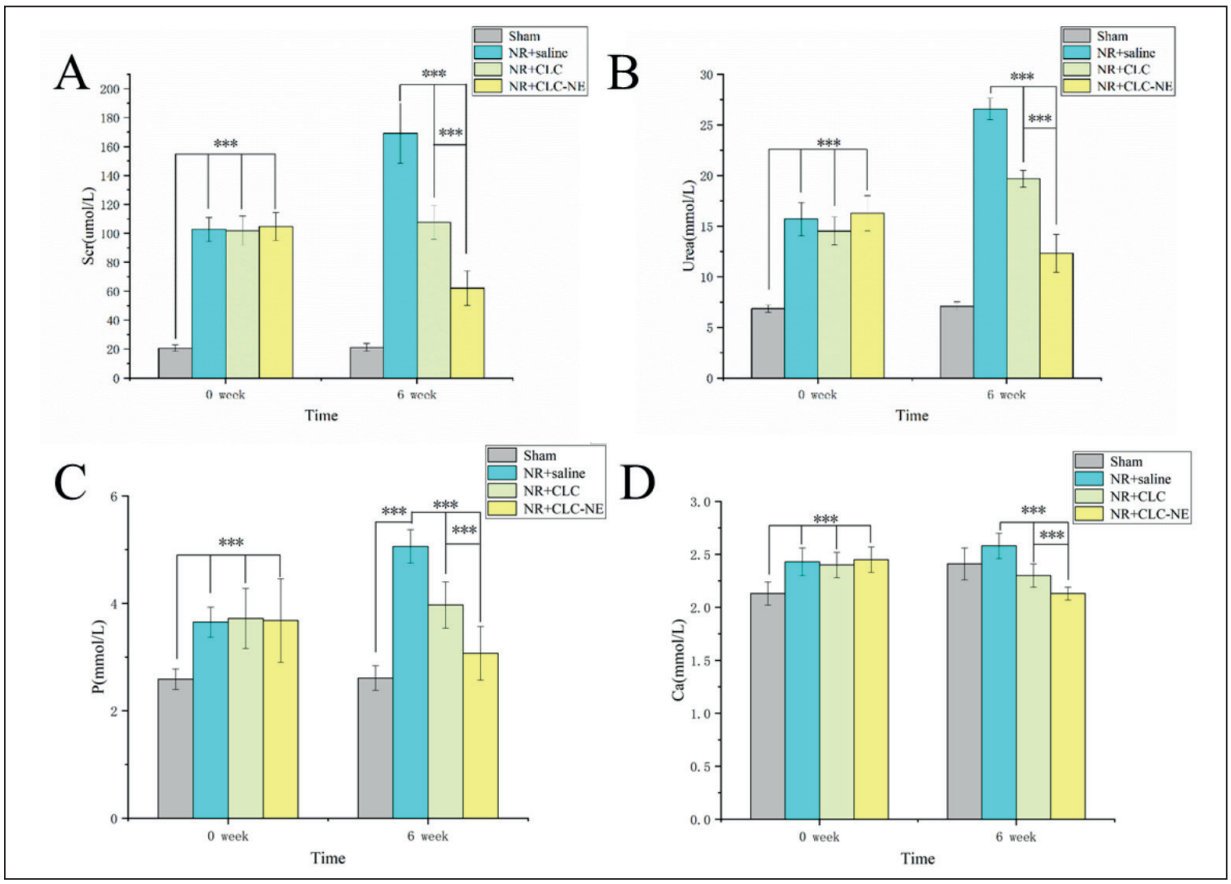

Figure 9. Changes of rats in different groups (Sham group, NR rats+ saline group, NR rats + CLC, NR rats + CLC-NE) during the 6-week treatment (Mean values ± SD, n=10, ***p<0.001). **A**, Scr; **B**, Urea; **C**, P; **D**, Ca.

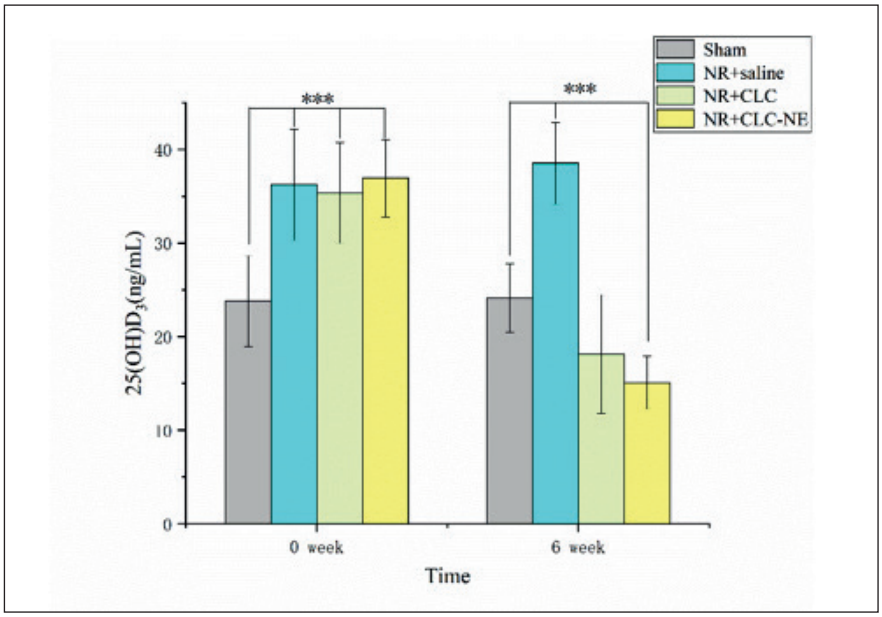

Figure 10. Effects of CLC-NE on serum 25(OH)D_3 of rats in different groups (Sham group, NR rats+ saline group, NR rats + CLC, NR rats + CLC-NE) during the 6-week treatment (Mean values ± SD, n=10, ***p<0.001).

tory effect (serum P level 3.07 mmol/L *vs.* 3.95 mmol/L) than CLC, suggesting that the renal function of NR was enhanced, and the rats could metabolize more P. At the same time, the serum content of Ca in NR also decreased (Figure 9D), which is also the clinical side effect of CLC.

Vitamin D_3 is synthesized in the skin, combined with vitamin Binding protein (DBP), and then, entered the liver. After 25-hydroxylation, 25(OH)D_3 is produced, which is the main circulating metabolite of vitamin D_3 and also the marker of the storage of vitamin D_3[44]. A 4-year investigation on non-hemodialysis patients with CKD showed that 25(OH)D_3 was an independent predictor of CKD progression and death[45], as the low metabolites of 25(OH)D_3 in the kidney could lead to parathyroid hyperplasia and aggravate SHPT[46].

After 6 weeks of continuous administration, the levels of serum 25(OH)D_3 in all rats were shown in Figure 10. The serum 25(OH)D_3 of rats in the NR+saline group was significantly higher than that of rats in the Sham group (35.35 ng/mL *vs.* 23.78 ng/mL), which was due to the impaired renal function of NR, causing the lack of 1α hydroxylase, resulting in the inability of 25(OH)D_3 to be converted into 1, 25$(OH)_2D_3$. The serum 25(OH)D3 of rats in the NR+CLC-NE group was significantly decreased (15.07 ng/mL), lower than that of rats in the Sham group (24.12 ng/mL), which was related to the improved renal function and the enhanced activity of 1α hydroxylase activity by CLC, corresponding to the decrease of Scr and Urea. Serum 25(OH)D3 of rats in the NR+CLC-NE group was lower than that of rats in the NR+ Saline group, which might be caused by the deficiency of vitamin D_3 in rats and the large conversion of 25(OH)D_3 to 1, 25$(OH)_2D_3$ stimulated by CLC.

FGF23 is a protein secreted by osteocytes and osteoblasts, which plays an important role in regulating the bone-parathyroid-renal axis and the metabolism of P[47]. After 5/6 of the kidneys were removed from NR, PTH could not regulate the serum P through the kidney, causing the increase of P, which can stimulate bone cells to produce excessive FGF23. Therefore, the serum FGF23 (2.53 ng/mL) and PTH (353.57 pg/mL) of NR were higher than those (0.99 ng/mL and 73.12 pg/mL) of rats in the Sham group (Figure 11A).

After the gastric administration of CLC-NE and CLC, the increasing FGF23 of NR was inhibited, which was significantly lower than that of the rats in the NR+saline group (5.04 ng/mL). Since CLC improves the renal function of rats, FGF23 can increase the excretion of P through urine and reduce the production of FGF23 by bone cells by inhibiting Na/P transporters in proximal convoluted tubules of the kidney. Due to the improvement of renal function of rats, FGF23 can also reduce the content of serum 1, 25$(OH)_2D_3$ and PTH by inhibiting lα-hydroxylase and stimulating 24-hy-

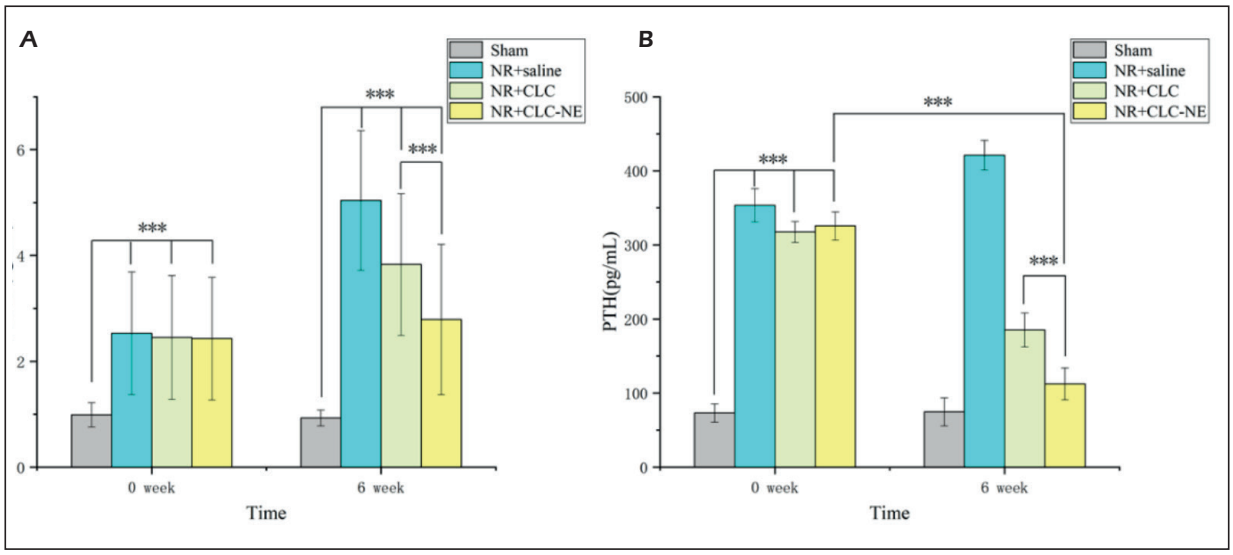

Figure 11. Effects of CLC-NE on serum FGF23 and PTH of rats in different groups (Sham group, NR rats+ saline group, NR rats + CLC, NR rats + CLC-NE, ***p<0.001).

droxylase, which is consistent with the decreased 25(OH) D_3 above.

Most importantly, FGF23 (2.79 ng/mL) and PTH (112.55 pg/mL) of NR with CLC-NE were significantly lower than those of NR with CLC (3.83 ng/mL and 185 pg/mL), suggesting that CLC-NE can better restore the renal function of NR, regulate the disordered endocrine of rats, and exert a stronger therapeutic effect on SHPT.

Discussion

The particle size of the nanoemulsion is generally between 10-100 nm with smaller PDI, indicating a more uniform particle size distribution. Through the solubility of CLC, we screened the oil phase, emulsifier, and co-emulsifier. CLC-NE was prepared through the phase inversion method with a particle size of 24.1±3.8 nm and PDI of 0.261±0.032, indicating the uniform particle size of CLC-NE. Due to the configuration of CLC-NE, as it is the O/W nanoemulsion with a water layer on its outer layer, which can exist stably in solution, CLC-NE can be stored stably for a long time.

Compared with REGPARA®, the relative bioavailability of CLC-NE was calculated to be 166.50%, which may be attributed to the significantly improved solubility of CLC after the preparation of CLC-NE. Meanwhile, the nanoemulsion also promoted the absorption of CLC by the gastrointestinal tract, further improving the bioavailability of CLC *in vivo*.

Due to the better absorption of CLC-NE, equal dose of CLC-NE can exert a stronger therapeutic effect than CLC on SHPT, as it can more effectively restore the renal function of NR rats, and regulate their endocrine, which was further confirmed in pharmacodynamics experiments.

Conclusions

The preparation of CLC-NE can improve the solubility, dissolution *in vitro,* and bioavailability *in vivo* of CLC, as well as the enhanced therapeutic effect on uremia rats. CLC-NE may be applied to the further research of CLC.

Ethics Approval

This study described was reviewed and approved by the Nanjing Medical University Institutional Animal Care and Use Committee (No. 202009107) and adhered to the ‘‘Principles of Laboratory Animal Care’’.

Conflicts of Interest

The authors state no conflict of interest.

Funding

This work was supported by the National Science and Technology Major Project (no.: 2019zx09301057).

Authors' Contributions

Jin Wang designed, carried out the experiment and wrote this article. Guoguang Chen and Lili Ren solved the problems encountered in the experiment and modified the paper.

ORCID ID

Jin Wang: https://orcid.org/0000-0002-4442-5719.

References

1) Ishaku SM, Olanrewaju TO, Browne JL, Klipstein-Grobusch K, Kayode GA. Prevalence and determinants of chronic kidney disease in women with hypertensive disorders in pregnancy in Nigeria: a cohort study. BMC Nephrol 2021; 22: 1-10.
2) Mallappallil MC, Fishbane S, Wanchoo R, Lerma E, Roche-Recinos A. Practice patterns in transitioning patients from chronic kidney disease to dialysis: a survey of United States nephrologists. BMC Nephrol 2018; 19: 1-7.
3) Ling XC, Kuo KL. Oxidative stress in chronic kidney disease. Korean J Transplant 2019; 4: 1-9.
4) Levey AS, Coresh J. Chronic kidney disease. Lancet Reg Health Am 2012; 379: 165-180.
5) Isaksson E, Ivarsson K, Akaberi S, Muth A, Prütz KG, Clyne, N, Almquist M. Total versus subtotal parathyroidectomy for secondary hyperparathyroidism. Surgery 2019; 165: 142-150.
6) Rose M, Shepherd J, Harris P, Pickett K, Lord J. Etelcalcetide for treating secondary hyperparathyroidism: an evidence review group evaluation of a nice single technology appraisal. Pharmacoecon 2018; 36: 1299-1308.
7) Saito T, Mizobuchi M, Hamada T, Sugiyama M, Miyazawa N, Morikawa T, Honda H. Tumoral calcinosis due to severe hyperphosphatemia and secondary hyperparathyroidism without vascular calcification in a hemodialysis patient. Clin Nephrol 2021; 95: 166.
8) Cook FJ, Seagrove-Guffey M, Mumm S, Veis DJ, McAlister WH, Bijanki VN, Whyte MP. Non-endemic skeletal fluorosis: Causes and associated secondary hyperparathyroidism (case report and literature review). Bone 2021; 145: 115839.
9) Sharanappa V, Pradhan S, Mishra A. Letter to editor in response to the article "Parathyroidectomy for patients with secondary hyperparathyroidism in a changing landscape for the management of end-stage renal disease" by Willemijn van der Plas et al published in Surgery. Surgery 2021; 169: 1262.
10) Carlo M, Gea I, Sandro F. Fp358paricalcitol therapy improves left ventricular hypertrophy in renal transplant patients with secondary hyperparathyroidism. Nep Dia Tra 2018; 33: i152-i152.
11) Siqueira FRD, Oliveira KCD, Dominguez WV, Truyts CAM, Moysés RMA, Dos Reis LM, Jorgetti V. Effect of parathyroidectomy on bone tissue biomarkers and body composition in patients with chronic kidney disease and secondary hyperparathyroidism. Eur J Clin Nutr 2021; 75: 1126-1133.
12) Yu JG, Song Y, Yang A, Zhang X, Li L. Serum nuclear factor IB as a novel and noninvasive indicator in the diagnosis of secondary hyperparathyroidism. J Clin Lab Anal 2021; 35: e23787.
13) Meyer HE, Falch JA, Søgaard AJ, Haug E. Vitamin D deficiency and secondary hyperparathyroidism and the association with bone mineral density in persons with Pakistani and Norwegian background living in Oslo, Norway: The Oslo Health Study. Bone 2004; 35: 412-417.
14) Mazziotti G, Lavezzi E, Brunetti A, Mirani M, Favacchio G, Pizzocaro A, Lania AG. Vitamin D deficiency, secondary hyperparathyroidism and respiratory insufficiency in hospitalized patients with COVID-19. J Endocrinol Invest 2021; 44: 2285-2293.
15) Peacock M, Bilezikian JP, Klassen PS, Guo MD, Turner SA, Shoback D. Cinacalcet hydrochloride maintains long-term normocalcemia in patients with primary hyperparathyroidism. J Clin Endocrinol Metab 2005; 90: 135-141.
16) Block GA, Zaun D, Smits G, Persky M, Brillhart S, Nieman K, St Peter WL. Cinacalcet hydrochloride treatment significantly improves all-cause and cardiovascular survival in a large cohort of hemodialysis patients. Kidney Int 2010; 78: 578-589.
17) Marotta V, Somma CD, Rubino M, Sciammarella C, Prete MD, Marciello F, Ramundo V, Circelli L, Buonomano P and Modica RJE. Potential role of cinacalcet hydrochloride in sporadic primary hyperparathyroidism without surgery indication. Endocrine 2015; 49: 274-278.
18) Moe SM, Chertow GM, Parfrey PS, Kubo Y, Block GA, Correa-Rotter R, Floege J. Cinacalcet, fibroblast growth factor-23, and cardiovascular disease in hemodialysis: the evaluation of cinacalcet HCl therapy to lower cardiovascular events (EVOLVE) trial. Circulation 2015; 132: 27-39.
19) Ketteler M, Martin KJ, Wolf M, Amdahl M, Cozzolino M, Goldsmith D, Khan S. Paricalcitol versus cinacalcet plus low-dose vitamin D therapy for the treatment of secondary hyperparathyroidism in patients receiving haemodialysis: results of the IMPACT SHPT study. Nephrol Dial Transpl 2012; 27: 3270-3278.
20) Ryšánek P, Grus T, Lukáč P, Kozlík P, Křížek T, Pozniak J, Slanař O. Validity of cycloheximide chylomicron flow blocking method for the evaluation of lymphatic transport of drugs. Brit J Pharmacol 2021; 178: 4663-4674.
21) Floege J, Tsirtsonis K, Iles J, Drueke TB, Chertow GM, Parfrey P. Incidence, predictors and therapeutic consequences of hypocalcemia in

patients treated with cinacalcet in the EVOLVE trial. Kidney Int 2018; 93: 1475-1482.

22) Agarwal H, Polaske TJ, Sánchez-Velázquez G, Blackwell HE, Lynn DM. Slippery nanoemulsion-infused porous surfaces (SNIPS): anti-fouling coatings that can host and sustain the release of water-soluble agents. Chem Commun 2021; 57: 12691-12694.

23) Carpenter AP, Foster MJ, Jones KK, Richmond GL. Effects of Salt-Induced Charge Screening on AOT Adsorption to the Planar and Nanoemulsion Oil–Water Interfaces. Langmuir 2021; 37: 8658-8666.

24) Shafaei N, Barkhordar SMA, Rahmani F, Nabi S, Idliki, RB, Alimirzaei M, Oskoueian E. Protective effects of Anethum graveolens Seed's oil Nanoemulsion against cadmium-induced oxidative stress in mice. Biol Trace Elem Res 2020; 198: 583-591.

25) O'Konek JJ, Landers JJ, Janczak KW, Lindsey HK, Mondrusov AM, Totten TD, Baker JR. Intranasal nanoemulsion vaccine confers long-lasting immunomodulation and sustained unresponsiveness in a murine model of milk allergy. Allergy 2020; 75: 872-881.

26) Qu Y, Li A, Ma L, Iqbal S, Sun X, Ma W, Ma D. Nose-to-brain delivery of disulfiram nanoemulsion in situ gel formulation for glioblastoma targeting therapy. Int J Pharm 2020; 597: 120250.

27) Qiu N, Liu Y, Liu Q, Chen Y, Huang LJB. Corrigendum to "Celastrol nanoemulsion induces immunogenicity and downregulates PD-L1 to boost abscopal effect in melanoma therapy". Biomaterials 2021; 277: 121121.

28) Rodrigues P, Ferrari FT, Barbosa LB, Righi A, Laporta L, Garlet QI, Heinzmann BM. Nanoemulsion boosts anesthetic activity and reduces the side effects of Nectandra grandiflora Nees essential oil in fish. Aquaculture 2021; 545: 737146.

29) Zeng B, Middelberg AP, Gemiarto A, MacDonald K, Baxter AG, Talekar M, Thomas, R. Self-adjuvanting nanoemulsion targeting dendritic cell receptor Clec9A enables antigen-specific immunotherapy. J Clin Invest 2018; 128: 1971-1984.

30) Wang C, Wu C, Zhang H, Lai J, Luo X, Liang Y, Tian J. Hydrothermal treatment of petrochemical sludge in subcritical and supercritical water: Oil phase degradation and syngas production. Chemosphere 2021; 278: 130392.

31) Zhu Y, Huan S, Bai L, Ketola A, Shi X, Zhang X, Rojas OJ. High internal phase oil-in-water pickering emulsions stabilized by chitin nanofibrils: 3D structuring and solid foam. ACS Appl Mater Inter 2020; 12: 11240-11251.

32) Gao Y, Wu X, Xiang Z, Qi C. Amphiphilic Double-Brush Copolymers with a Polyurethane Backbone: A Bespoke Macromolecular Emulsifier for Ionic Liquid-in-Oil Emulsion. Langmuir 2021; 37: 2376-2385.

33) Léonard-Akkari L, Guégan S, Courand F, Couvert O, Lepage JF, Rondeau-Mouro C, Decourcelle N. Dispersed phase volume fraction, weak acids and Tween 80 in a model emulsion: Effect on the germination and growth of Bacillus weihenstephanensis KBAB4 spores. Food Res Int 2018; 109: 288-297.

34) Feng SM, Zhao Y, Xu Q, Li HM, Huang YX, Liu HH, Xu CB. Development and Characterization of A New Dimethicone Nanoemulsion and its Application for Electronic Gastroscopy Examination. Int J Nanomed 2020; 15: 5405.

35) Karcher V, Perrechil FA, Bannwart AC. Interfacial energy during the emulsification of water-in-heavy crude oil emulsions. Braz J Chem Eng 2015; 32: 127-137.

36) Hua C, Chen K, Wang Z, Guo X. Preparation, stability and film properties of cationic polyacrylate latex particles with various substituents on the nitrogen atom. Prog Org Coat 2020; 143: 105628.

37) Ahmad A, Amir M, Alshadidi AA, Hussain MD, Haq A, Kazi M. Central composite design expert-supported development and validation of HPTLC method: Relevance in quantitative evaluation of protopine in Fumaria indica. Saudi Pharm J 2020; 28: 487-494.

38) An T, Choi J, Kim A, Lee JH, Nam Y, Park J, Hwang SJ. Sustained release of risperidone from biodegradable microspheres prepared by in-situ suspension-evaporation process. Int J Pharm 2016; 503: 8-15.

39) Viennois E, Merlin D, Gewirtz AT, Chassaing B. Dietary emulsifier–induced low-grade inflammation promotes colon carcinogenesis. Cancer Res 2017; 77: 27-40.

40) Ebrahimi S, Hasanzadeh-Barforoushi A, Nejat A, Kowsary F. Numerical study of mixing and heat transfer in mixed electroosmotic/pressure driven flow through T-shaped microchannels. Int J Heat Mass Tran 2014; 75: 565-580.

41) Pickup L, Loutradis C, Law JP, Arnold JJ, Dasgupta I, Sarafidis P, Ferro CJ. The effect of admission and pre-admission serum creatinine as baseline to assess incidence and outcomes of acute kidney injury in acute medical admissions. Nephrol Dial Transpl 2022; 37: 148-158.

42) Angeloco LRN, Arces de Souza GC, Romão EA, Frassetto L, Chiarello PG. Association of dietary acid load with serum bicarbonate in chronic kidney disease (CKD) patients. Eur J Clin Nutr 2020; 74: 69-75.

43) Chasapi A, Balampanis K, Tanoglidi A, Kourea E, Lambrou GI, Lambadiari V, Sotiropoulou-Bonikou G. Src-3/aib-1 may enhance hepatic nfatc1 transcription and mediate inflammation in a tissue-specific manner in morbid obesity. Endocrine 2020; 20: 242-255.

44) Castillo-Peinado LS, Calderón-Santiago M, Priego-Capote F. Lyophilization as pre-processing for sample storage in the determination of vitamin D3 and metabolites in serum and plasma. Talanta 2021; 222: 121692.

45) Chen SW, Wang PY, Zhu J, Chen GW, Zhang JL, Chen ZY, Pan YS. Protective effect of 1, 25-dihydroxyvitamin d3 on lipopolysaccharide-induced intestinal epithelial tight junction injury in caco-2 cell monolayers. Inflammation 2015; 38: 375-383.

46) Heureux N. Vitamin D testing—where are we and what is on the horizon. Adv Clin Chem 2017; 78: 59-101.

47) Alber J, Föller M. Lactic acid induces fibroblast growth factor 23 (FGF23) production in UMR106 osteoblast-like cells. Mol Cell Biochem 2022; 477: 363-370.